MICROWAVE EMISSION MODEL FOR WET SNOW BY USING RADIATIVE TRANSFER AND STRONG FLUCTUATION THEORY

H. Wang

Nokia Mobile Phones
P.O. Box 83 (Sinitaival 5)
FIN-33721 Tampere, Finland

A. N. Arslan

Nokia Research Center
P.O. Box 407
FIN-00045 NOKIA GROUP, Finland

J. Pulliainen and M. Hallikainen

Laboratory of Space Technology
P.O. Box 3000
FIN-02015, HUT, Finland

Abstract–This study is concerned with the development of a model to describe microwave emission from terrain covered by wet snow. The model is based on the radiative transfer theory and the strong fluctuation theory. Wet snow is treated in the model as a mixture of dry snow and water inclusions. The shape of the water inclusions is taken into account. The effective permittivity is calculated by using the two-phase strong fluctuation theory model with nonsymmetrical inclusions. The phase matrix and the extinction coefficient of wet snow for an anisotropic correlation function with azimuth symmetric are used. The vector radiative transfer equation for a layer of a random medium was solved by using Gaussian quadrature and eigen analysis. The model behaviour is illustrated by using typical parameters encountered in microwave remote sensing of wet snow. Comparisons with emissivity data at 11, 21 and 35 GHz are made. It is shown that the model predictions fit the experimental data.

1. INTRODUCTION

Snow can be divided into two categories: dry snow and wet snow. Refrozen snow is dry snow that has gone through several melt-froze cycles. Passive microwave remote sensing of dry snow has been studied extensively by using semi-empirical models [1, 2] or theoretical models including strong fluctuation approach [3–5], radiation transfer with discrete scatterers [6–8] and dense media radiation transfer equations [9, 10]. However, the experimental and theoretical studies of wet snow are still very limited [3, 11–14]. The purpose of this study is to develop a model to describe microwave emission from wet snow, based on the radiative transfer theory and the strong fluctuation theory.

When melting begins, snow wetness becomes the major parameter defining the emission properties of the soil-snow-atmosphere system [12]. The brightness temperature of wet snow is strongly influenced by its free water content. Therefore, wet snow can be treated as a two-phase mixture by considering the water particles as inclusions embedded in dry snow that is the background medium. Under this assumption, it is important to consider the shape of the water inclusions. In this study, an anisotropic and azimuth symmetric correlation function is used which correspond to sphere, needle or disk-like shape, when the two correlation lengths are treated with different values [4, 15].

A good summary of the semi-empirical dielectric models of wet snow is found in Hallikainen et al. [16]. The effective permittivity of wet snow can also be calculated by using the strong fluctuation theory. Jin and Kong attempted to use the strong fluctuation theory with a three-phase mixture (air, spherical ice particles, and spherical water particles) to calculate the permittivity of wet snow [17]. Our previous work has shown that consideration of the shape of inclusions is important and the two-phase model with nonsymmetrical inclusions provided better results than that three-phase model with spherical inclusions for the effective permittivity of wet snow [18].

In this paper the phase matrix and extinction coefficient of wet snow are calculated by using the strong fluctuation theory for an azimuthally symmetric correlation function [4, 15]. Unfortunately, the expressions for the effective permittivity and the coefficient $\overline{\overline{S}}$ of the delta function in mean dyadic Greens function are not identical in [4] and [15]. The key point is that they used a different method to evaluate the principal value of the dyadic Greens function. We will adopt the coefficient $\overline{\overline{S}}$ according to [4] in our model.

We solve the vector radiative transfer equation for a layer of a random medium by using Gaussian quadrature and eigen analysis. Comparisons with literature-based brightness temperature data [14] at 11, 21 and 35 GHz are made.

2. THE EFFECTIVE PERMITTIVITY OF WET SNOW

The effective permittivity tensor $\overline{\overline{\varepsilon}}_{eff}$ of wet snow has been studied in our previous paper [18]. For easy reference, we give the main formulations of our wet snow effective permittivity model in this section.

In our model, wet snow is treated as a two phase-mixture by considering the water particles as inclusions embedded in dry snow that is the background material as shown in Fig. 1. The permittivity of the scatterers is $\varepsilon_s = \varepsilon_{water}$ and the permittivity of the background medium is $\varepsilon_b = \varepsilon_{dry\_snow}$. The fraction volume occupied by the water inclusions is f_ν and the fraction volume occupied by the dry snow is $1 - f_\nu$. The shape of the water inclusions is considered by using an anisotropic and azimuthally symmetric correlation function [4, 15]:
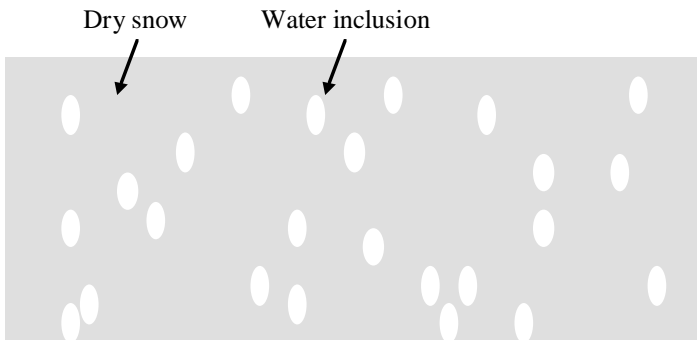
Figure 1. Wet snow as a two-phase mixture.

$$ACF(r) = \exp\left(-\frac{x^2 + y^2}{l_\rho^2} - \frac{|z|}{l_z}\right), \tag{1}$$

where $l_\rho = l_x = l_y$ is the correlation length in horizontal direction and l_z is the correlation length in vertical direction.

The elements of the uniaxial effective permittivity tensor $\overline{\overline{\varepsilon}}_{eff} = diag\left[\varepsilon_{effp} \ \varepsilon_{effp} \ \varepsilon_{effz}\right]$ for an anisotropic and azimuthally symmetric correlation function are given by [15, 19–21]:

$$\varepsilon_{effp} = \varepsilon_g + \frac{\varepsilon_0 \delta_{11}(I_1 + S)}{1 - S\delta_{11}(I_1 + S)} \tag{2}$$

$$\varepsilon_{effz} = \varepsilon_{gz} + \frac{\varepsilon_0 \delta_{33}(I_3 + S_z)}{1 - S_z\delta_{33}(I_3 + S_z)}, \tag{3}$$

where ε_g and ε_{gz} are the quasi-static permittivity in horizontal and vertical direction, respectively. They are the solutions of two non-linear coupled equations [4]:

$$f_\nu \cdot \frac{\varepsilon_s - \varepsilon_g}{\varepsilon_0 + S(\varepsilon_s - \varepsilon_g)} + (1 - f_\nu) \cdot \frac{\varepsilon_b - \varepsilon_g}{\varepsilon_0 + S(\varepsilon_b - \varepsilon_g)} = 0 \tag{4}$$

$$f_\nu \cdot \frac{\varepsilon_s - \varepsilon_{gz}}{\varepsilon_0 + S_z(\varepsilon_s - \varepsilon_{gz})} + (1 - f_\nu) \cdot \frac{\varepsilon_b - \varepsilon_{gz}}{\varepsilon_0 + S_z(\varepsilon_b - \varepsilon_{gz})} = 0. \tag{5}$$

S and S_z in equations (2) and (3) are the dyadic coefficient of the Dirac delta part in the dyadic Greens function of an anisotropic medium [4],

$$S = \frac{\varepsilon_0 \cdot b_1^{1/2}}{\varepsilon_g \left(2b_1^{1/2} + 1\right)} \tag{6}$$

$$S_z = \frac{\varepsilon_0}{\varepsilon_{gz} \left(2b_1^{1/2} + 1\right)} \tag{7}$$

$$b_1 = \frac{\varepsilon_g \cdot l_z^2}{\varepsilon_{gz} \cdot l_\rho^2}. \tag{8}$$

The variances δ_{11} and δ_{33} in equations (2) and (3) are deduced from ε_g and ε_{gz} [15]:

$$\delta_{11} = f_\nu \cdot \left|\frac{\varepsilon_s - \varepsilon_g}{\varepsilon_0 + S(\varepsilon_s - \varepsilon_g)}\right|^2 + (1 - f_\nu) \cdot \left|\frac{\varepsilon_b - \varepsilon_g}{\varepsilon_0 + S(\varepsilon_b - \varepsilon_g)}\right|^2 \tag{9}$$

$$\delta_{33} = f_\nu \cdot \left|\frac{\varepsilon_s - \varepsilon_{gz}}{\varepsilon_0 + S_z(\varepsilon_s - \varepsilon_{gz})}\right|^2 + (1 - f_\nu) \cdot \left|\frac{\varepsilon_b - \varepsilon_{gz}}{\varepsilon_0 + S_z(\varepsilon_b - \varepsilon_{gz})}\right|^2. \tag{10}$$

The integrals I_1 and I_3 in equations (2) and (3) for the correlation function (1) can be written as [15]:

$$
\begin{aligned}
I_1 = & -\frac{\sqrt{\varepsilon_{gz}\varepsilon_0}}{2\pi h \varepsilon_g^{3/2}} \int_0^{\pi/2} d\theta \sin\theta \tan^2\theta \cdot \left\{ \sqrt{\pi} - \pi \frac{\tan\theta}{2h\sqrt{b}} \exp\left(\frac{\tan^2\theta}{4h^2 b}\right) \right. \\
& \left. \cdot erfc\left(\frac{\tan\theta}{2h\sqrt{b}}\right) \right\} + \frac{k_0^2 l_\rho^2}{4} \frac{\varepsilon_{gz}}{\varepsilon_g} \int_0^{\pi/2} d\theta \sin\theta \cos\theta \exp\left(\frac{\tan^2\theta}{4h^2 b}\right) \\
& \cdot erfc\left(\frac{\tan\theta}{2h\sqrt{b}}\right) + \frac{k_0^2 l_\rho^2}{8} \int_0^{\pi/2} d\theta \tan\theta \exp\left(\frac{\tan^2\theta}{4h^2}\right) \\
& \cdot erfc\left(\frac{\tan\theta}{2h}\right) + \frac{i k_0^3 l_\rho^2 l_z}{12} \frac{\varepsilon_{gz}}{\sqrt{\varepsilon_g \varepsilon_0}} + \frac{i k_0^3 l_\rho^2 l_z}{3} \sqrt{\frac{\varepsilon_g}{\varepsilon_0}} \quad (11)
\end{aligned}
$$

$$
\begin{aligned}
I_3 = & -\frac{\varepsilon_0}{\sqrt{\varepsilon_{gz}\varepsilon_g}} \frac{1}{\pi h} \int_0^{\pi/2} d\theta \left\{ \sqrt{\pi} - \pi \frac{\tan\theta}{2h\sqrt{b}} \exp\left(\frac{\tan^2\theta}{4h^2 b}\right) \right. \\
& \left. \cdot erfc\left(\frac{\tan\theta}{2h\sqrt{b}}\right) \right\} + \frac{k_0^2 l_\rho^2}{2} \int_0^{\pi/2} d\theta \sin^2\tan\theta \exp\left(\frac{\tan^2\theta}{4h^2 b}\right) \\
& \cdot erfc\left(\frac{\tan\theta}{2h\sqrt{b}}\right) + \frac{i k_0^3}{3} l_\rho^2 l_z \sqrt{\frac{\varepsilon_g}{\varepsilon_0}} \quad (12)
\end{aligned}
$$

where $b = \frac{\varepsilon_g}{\varepsilon_{gz}}$, $h = \frac{l_z}{l_\rho}$; and *erfc* is an incomplete error function with complex arguments:

$$
erfc(z) = 1 - erf(z) = 1 - \frac{2}{\sqrt{\pi}} \int_0^z e^{-z^2} dt. \quad (13)
$$

3. THE BRIGHTNESS TEMPERATURE OF WET SNOW

Our microwave emission model for wet snow is based on the solution of the radiative transfer equation inside the snowpack by taking into account the boundaries at the soil and atmosphere interfaces, as shown in Figure 2.

Inside an inhomogeneous medium, let $T_\nu(\theta, z)$ and $T_h(\theta, z)$ denote brightness temperatures at vertical and horizontal polarisation. The radiation transfer equations for passive remote sensing can be written as [6]:

$$
\begin{aligned}
\cos\theta \frac{d}{dz} \begin{bmatrix} T_\nu(\theta, z) \\ T_h(\theta, z) \end{bmatrix} = & \kappa_a T_1(z) - \begin{bmatrix} \kappa_{e\nu} T_\nu(\theta, z) \\ \kappa_{eh} T_\nu(\theta, z) \end{bmatrix} \\
& + \int_0^\pi d\theta' \sin\theta' \begin{bmatrix} P_{11}(\theta, \theta') & P_{12}(\theta, \theta') \\ P_{21}(\theta, \theta') & P_{22}(\theta, \theta') \end{bmatrix} \begin{bmatrix} T_\nu(\theta', z) \\ T_h(\theta', z) \end{bmatrix}, \quad (14)
\end{aligned}
$$
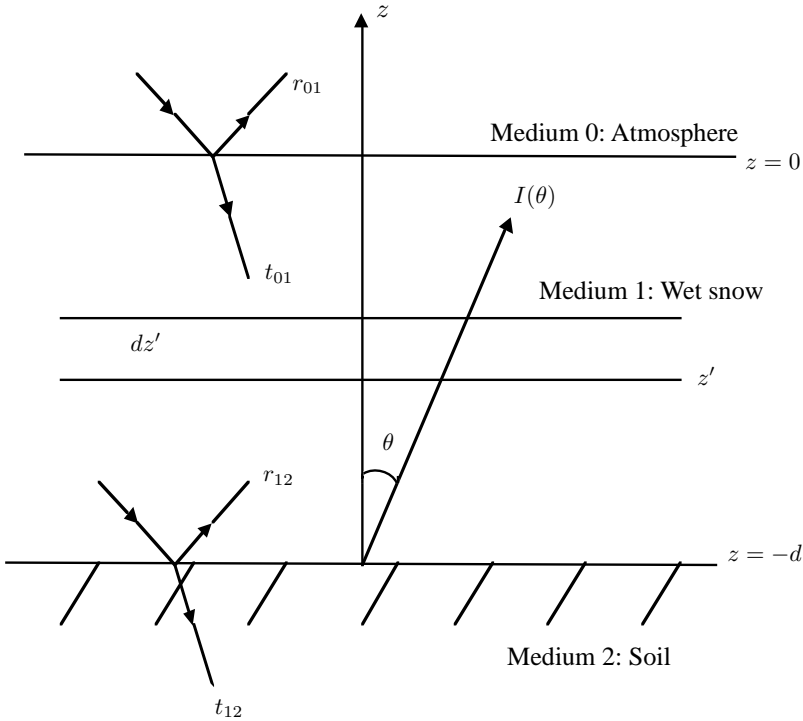
Figure 2. Geometrical configuration of a three-layer medium.

where κ_a is the absorption coefficient, $\kappa_{ep} = \kappa_a + \kappa_{sp}$ $(p = \nu, h)$ is the p-polarised extinction coefficient and κ_{sp} is the scattering coefficient. θ is the incidence angle, θ' is the scattering angle, $T_1(z)$ is the temperature profile of the inhomogeneous layer, and $P_{11}(\theta, \theta')$, $P_{12}(\theta, \theta')$ $P_{21}(\theta, \theta')$ and $P_{22}(\theta, \theta')$ are the phase matrix elements.

The absorption coefficient κ_a is expressed as [22]:

$$\kappa_a = 2k_0 \text{Im} \left\lfloor \varepsilon_{gwet}^{1/2} \right\rfloor, \tag{15}$$

where k_0 is the wave number in free space, and ε_{gwet} is the quasi-static value of the dielectric constant of wet snow. The scattering coefficients $\kappa_{s\nu}$ and κ_{sh} are deduced from the phase matrix components $P(\theta, \phi; \theta', \phi')$ [4]:

$$\kappa_{s\nu}(\theta) = \int_0^\pi d\theta' \sin \theta' \left[P_{11}(\theta, \theta') + P_{21}(\theta, \theta') \right] \tag{16}$$

$$\kappa_{sh}(\theta) = \int_0^\pi d\theta' \sin\theta' \left[P_{12}(\theta, \theta') + P_{22}(\theta, \theta') \right] \qquad (17)$$

The elements of the phase matrix for the transverse isotropic correlation functions (1) can be written as [4]:

$$P_{11}(\theta, \ \theta') = Q(\theta - \theta') \exp(-A) \left\{ \left[\delta_{33} \sin^2\theta \sin^2\theta' + \frac{1}{2}\delta_{11} \cos^2\theta \cos^2\theta' \right] I_0(A) \right.$$

$$\left. + 2\delta_{13} \sin\theta \sin\theta' \cos\theta \cos\theta' I_1(A) \frac{1}{2}\delta_{11} \cos^2\theta \cos^2\theta' I_2(A) \right\} (18)$$

$$P_{12}(\theta, \ \theta') = \frac{1}{2}\delta_{11} Q(\theta, \ \theta') \exp(-A) \cos^2\theta [I_0(A) - I_2(A)] \qquad (19)$$

$$P_{12}(\theta, \ \theta') = \frac{1}{2}\delta_{11} Q(\theta, \ \theta') \exp(-A) \cos^2\theta' [I_0(A) - I_2(A)] \qquad (20)$$

$$P_{22}(\theta, \ \theta') = \frac{1}{2}\delta_{11} Q(\theta, \ \theta') \exp(-A)[I_0(A) + I_2(A)], \qquad (21)$$

where

$$Q(\theta, \ \theta') = \frac{k_{wet}^4}{4} \frac{l_z l_\rho^2}{1 + k_{wet}^2(\cos\theta - \cos\theta')^2 l_z^2} \exp\left[-\frac{k_{wet}^2 l_\rho^2 (\sin\theta - \sin\theta')^2}{4} \right]$$

$$\tag{22}$$

$$A = \frac{k_{wet}^2 l_\rho^2 \sin\theta \sin\theta}{2}, \qquad (23)$$

where $I_n(A)$ is the modified Bessel Function of the first kind of n-th order, and k_{wet} is the wave number in wet snow

$$k_{wet} = \omega\sqrt{\mu\varepsilon_{eff}} = k_0\sqrt{\frac{\varepsilon_{eff}}{\varepsilon_0}}, \qquad (24)$$

where ε_{eff} is the effective permittivity of wet snow.

The radiative transfer equation (14) can be solved by using Gaussian quadrature and eigenanalysis technique subject to the following boundary conditions, for $0 < \theta < \pi/2$ [23]:

$$T_p(\theta, z = -d) = r_{12p}(\theta)T_p(\pi - \theta, z = -d) + t_{12p}(\theta)T_{soil} \quad (25)$$

$$T_p(\pi - \theta, z = 0) = r_{01p}(\theta)T_p(\theta, z = 0) + t_{01p}(\theta)T_{skyp}(\theta_0), \quad (26)$$

where r_{12p}, r_{01p} are reflectivities, t_{12p}, t_{01p} are transmissivities, and $t_{mnp} = 1 - r_{mnp} \cdot \theta$ and θ_0, and θ and θ_2 are related by Snells law, respectively.

In the calculation of the reflectivity, the effective permittivity of dry snow, wet snow and soil should be known. In this study, the Stogryn's model in [24] and [25] is used to calculate the effective permittivity of dry snow. The measured permittivity and dielectric loss factor of soil as a function of frequency and with temperature as a parameter can be obtained from [26].

The sky radiation is approximated by [23]:

$$T_{sky\,p}(\theta_0) = T_{air}[1 - \exp(-k_{0a} \cdot t \cdot \sec\theta_0)] \tag{27}$$

with T_{air} denoting the air temperature, k_{0a} the absorption coefficient of the air, and t the thickness of the atmosphere.

Once the radiation transfer equation (14) is solved subject to the boundary conditions (25) and (26), the brightness temperatures are given by [23]:

$$T_B(\theta_0) = t_{01\,p}(\theta)T_p(\theta, z = 0) + r_{01\,p}(\theta_0)T_{sky\,p}(\theta_0). \tag{28}$$

To find a possible effect due to the small roughness of the surface, we simply modify the reflectivity r_{mnp} according to [4]:

$$r_{mnp1} = \exp\left(-h\cos^2\theta\right) r_{mnp}, \tag{29}$$

where h is the effective roughness.

It should be noted that the quasi-static permittivity $\bar{\bar{\varepsilon}}_g$ and the effective permittivity $\bar{\bar{\varepsilon}}_{eff}$ of wet snow are uniaxial tensors as we discussed in Section 2. For simplicity, we use an isotropic value of the quasi-static permittivity ε_{gwet} instead of $\bar{\bar{\varepsilon}}_g$ in the equations of the absorption coefficient (15), and an isotropic value of the effective permittivity ε_{eff} instead of $\bar{\bar{\varepsilon}}_{eff}$ in the phase matrix element (18) to (24). In the calculation of the reflectivities $r_{12\,p}$, $r_{01\,p}$ and the transmissivities $t_{12\,p}$, $t_{01\,p}$, an isotropic value of the effective permittivity ε_{eff} is also used instead of the uniaxial tensor $\bar{\bar{\varepsilon}}_{eff}$. In the case of wet snow, the vertical direction is dominant. In the following calculation, we set:

$$\varepsilon_{gwet} = \varepsilon_{gz} \tag{30}$$

$$\varepsilon_{eff} = \varepsilon_{effz}. \tag{31}$$

The model needs to be further studied concerning the use of the uniaxial tensors $\bar{\bar{\varepsilon}}_g$ and $\bar{\bar{\varepsilon}}_{eff}$ throughout the calculations.

4. PERFORMANCE OF THE MODEL

In order to illustrate the model behaviour, we shall consider the dependence of the emissivity of wet snow on the input parameters in this section.

The model flow chart is shown in Figure 3. The input parameters of our emission model for wet snow are the measurement frequency f, the temperature of wet snow T, the depth of wet snow H, the mean grain size of ice particles D_{ice}, the volume fraction of ice particles f_{ν_ice}, the volume fraction of water inclusions f_{ν_water} and the correlation lengths in vertical and horizontal direction of water inclusions l_ρ, l_z. In the model, the ice permittivity ε_{ice} is calculated from the model [27] or [28]. The dry snow permittivity $\varepsilon_{dry-snow}$ is calculated from the model [24] and [25]. The complex permittivity of free water with no salinity ε_{water} can be described by Debye equation [29]
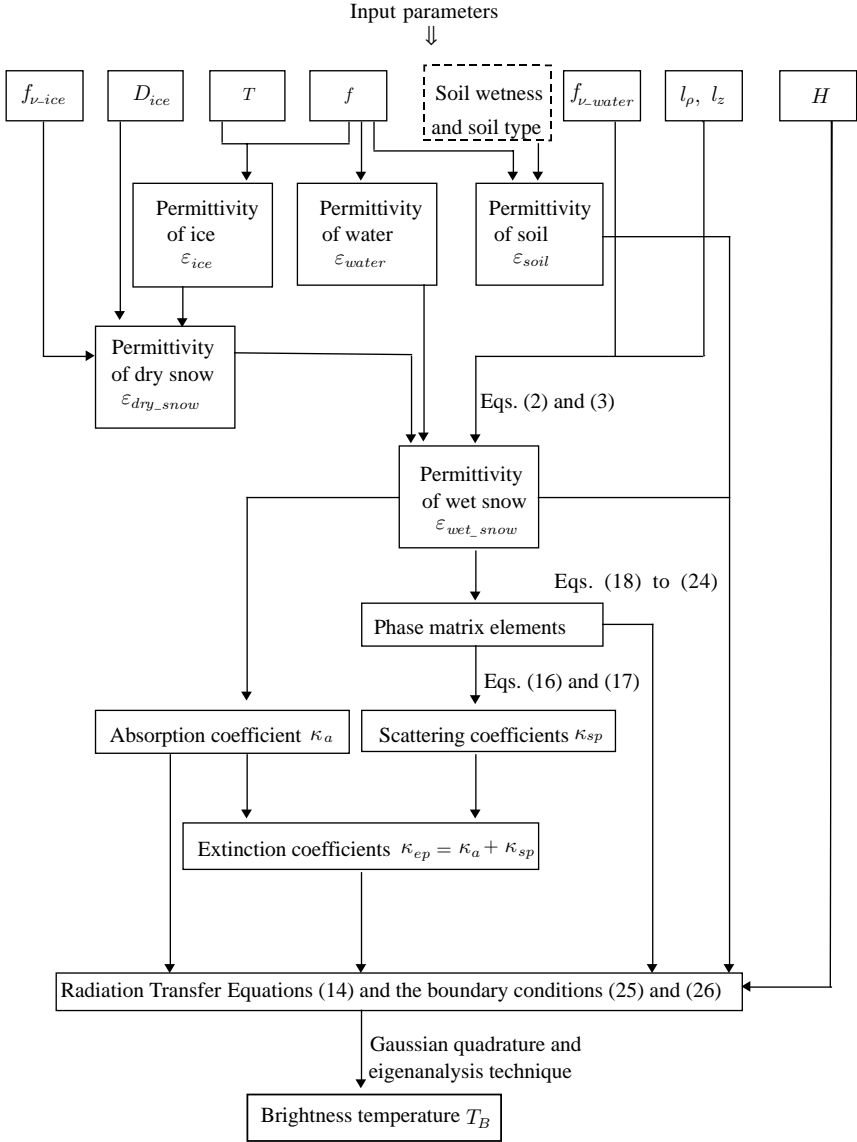
$$\varepsilon_{water} = \varepsilon_{\infty w} + \frac{\varepsilon_{sw} - \varepsilon_{\infty w}}{1 - if/f_{0k}}, \tag{32}$$

where the static permittivity ε_{sw}, the optical permittivity $\varepsilon_{\infty w}$ and the relaxation frequency f_{0k} of liquid water at $T = 0°\,\mathrm{C}$ are chosen ($\varepsilon_{sw} = 88$, $\varepsilon_{\infty w} = 4.9$ and $f_{0k} = 9\,\mathrm{GHz}$). The permittivity of soil ε_{soil} is obtained from [26].

The basic set of input parameters for the calculations of this section is listed in Table 1. The volume fraction of water inclusions is set to be $f_{\nu\_water} = 0.05$. The correlation lengths of water inclusions are often selected to match the theoretical results into the observations. However, here we used the correlation lengths of water inclusions according to our previous study of wet snow permittivity [18]; the values of the correlation lengths of water inclusions in vertical and horizontal direction are $l_\rho = 0.11\,\mathrm{mm}$ and $l_z = 0.43\,\mathrm{mm}$. These values provide a good match between the results of the permittivity model of wet snow and the observations when the volume fraction of water inclusions is $f_{\nu\_water} = 0.05$. Later we will show that these values for the correlation lengths enable the results of the brightness temperature model of wet snow to match the observations as well.

Table 1. The basic set of input parameters.

f (GHZ)	T (K)	H (mm)	f_{ν_ice}	D_{ice} (mm)	f_{ν_water}	l_ρ (mm)	l_z (mm)
11,21,35	273	810	0.3	0.8	0.05	0.11	0.43

Input parameters
⇓

| $f_{\nu-ice}$ | D_{ice} | T | f | Soil wetness and soil type | f_{ν_water} | l_ρ, l_z | H |

Permittivity of ice ε_{ice}

Permittivity of water ε_{water}

Permittivity of soil ε_{soil}

Permittivity of dry snow ε_{dry_snow}

Eqs. (2) and (3)

Permittivity of wet snow ε_{wet_snow}

Eqs. (18) to (24)

Phase matrix elements

Eqs. (16) and (17)

Absorption coefficient κ_a

Scattering coefficients κ_{sp}

Extinction coefficients $\kappa_{ep} = \kappa_a + \kappa_{sp}$

Radiation Transfer Equations (14) and the boundary conditions (25) and (26)

Gaussian quadrature and eigenanalysis technique

Brightness temperature T_B

Figure 3. Model structure. See the text for detailed descriptions of input parameters and various modules.

The mean grain size and the volume fraction of ice particles are used only to calculate the effective permittivity of dry snow, and the realistic values of the grain size of ice particles $D_{ice} = 0.08\,\text{mm}$ and the volume
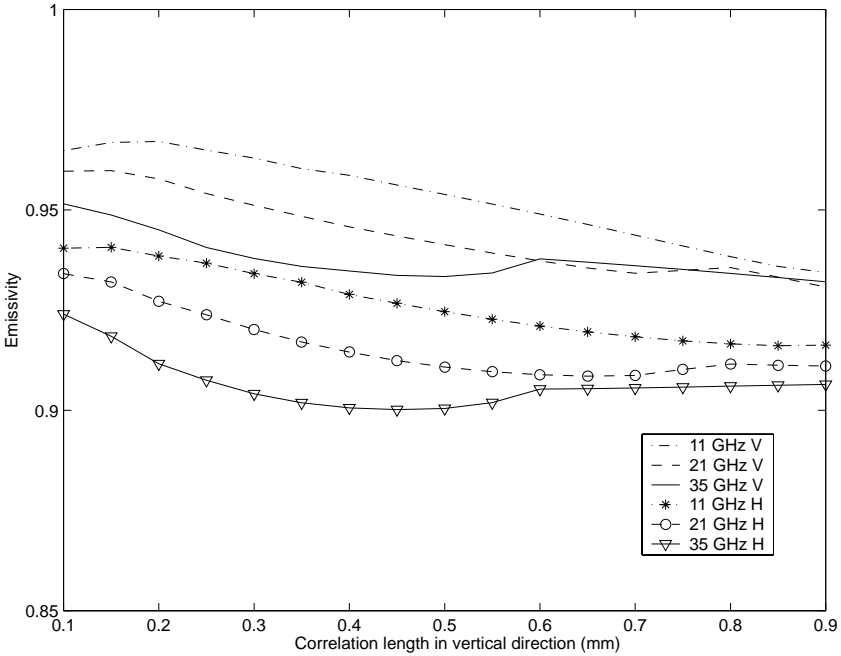
Figure 4. Theoretical wet snow emissivity as a function of the correlation length in vertical direction l_z. The correlation length in horizontal direction l_ρ is set to be $0.4\,\text{mm}$ and the observation angle is $50°$. See Table 1 for other input parameters.

fraction of ice particles $f_{\nu\_ice} = 0.3$ are used in the model.

Figures 4 to 6 show the effect of the size and shape of water inclusions on wet snow emissivity. In Figure 4, the correlation length in horizontal direction l_ρ is set to be $0.4\,\text{mm}$, the correlation lengths in vertical direction l_z changes from $0.1\,\text{mm}$ to $0.9\,\text{mm}$. The observation angle is $50°$. Figure 4 shows that when the water inclusions are disk-like or spherical in shape, $l_z \leq l_\rho(0.4\,\text{mm})$, wet snow emissivity decreases with increasing frequency. With the water inclusions turned to be cylinder-like in shape, $l_z > l_\rho(0.4\,\text{mm})$, the decrease in wet snow emissivity with increasing frequency becomes smaller. However, when the correlation length in horizontal direction l_ρ is very small and the water inclusions are cylinder-like in shape, $l_z > l_\rho(0.1\,\text{mm})$, the wet snow emissivities at all three frequencies are almost same, and the effect of changes in the correlation lengths in vertical direction l_z in negligible, as shown in Figure 5.
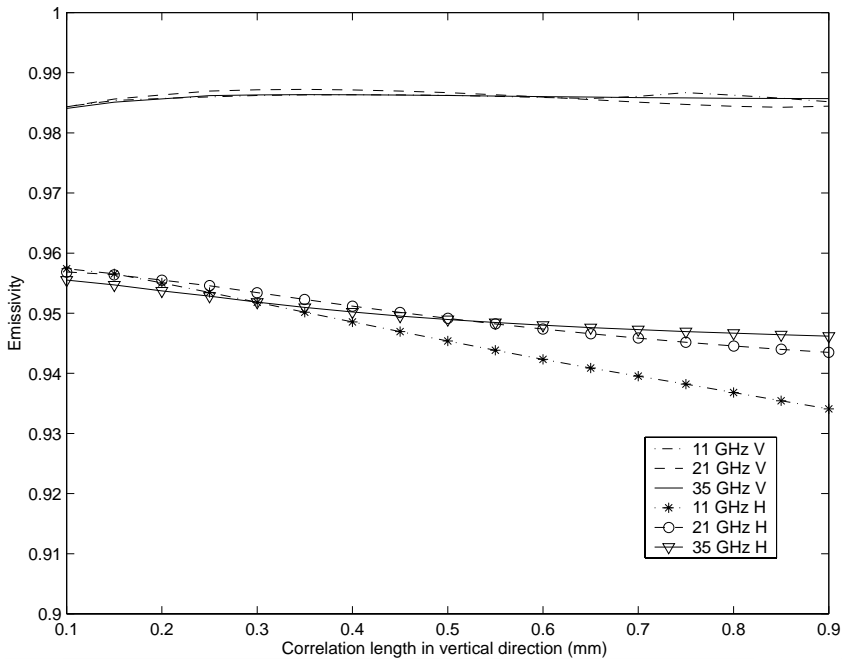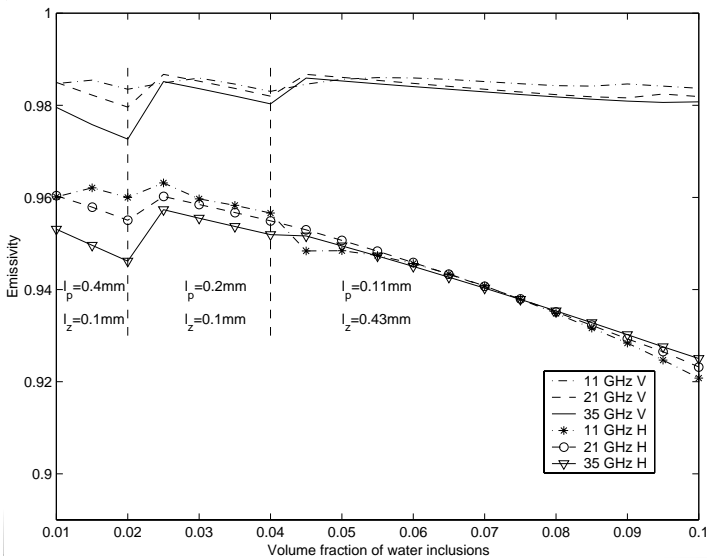
Figure 5. Theoretical wet snow emissivity as a function of the correlation length in vertical direction l_z. The correlation length in horizontal direction l_ρ is set to be $0.1\,\mathrm{mm}$ and the observation angle is $50°$. See Table 1 for other input parameters.

In Figure 6, the correlation length in vertical direction l_z is set to be $0.4\,\mathrm{mm}$, the correlation lengths in horizontal direction l_ρ changes from $0.1\,\mathrm{mm}$ to $1\,\mathrm{mm}$. The observation angle is $50°$. Figure 6 shows that wet snow emissivity decreases with increasing the correlation length in vertical direction l_z. With increasing frequency, wet snow emissivity decreases.

Figure 7 shows the theoretical results of wet snow emissivity as a function of the volume fraction of water inclusions (the liquid water content). The observation angle is $50°$. According to [16], the water inclusions in wet snow appear needle-like in shape for the volume fraction below $f_\nu = 0.03$. However, they become disk-like for $f_\nu \geq 0.03$. This change in shape appears to be due to the transition from the pendular regime to the funicular regime. But in this paper, water inclusions are disk-like in shape for the volume fraction below $f_\nu = 0.04$. The correlation lengths are selected to be $l_z = 0.01\,\mathrm{mm}$ and $l_\rho = 0.4\,\mathrm{mm}$ when
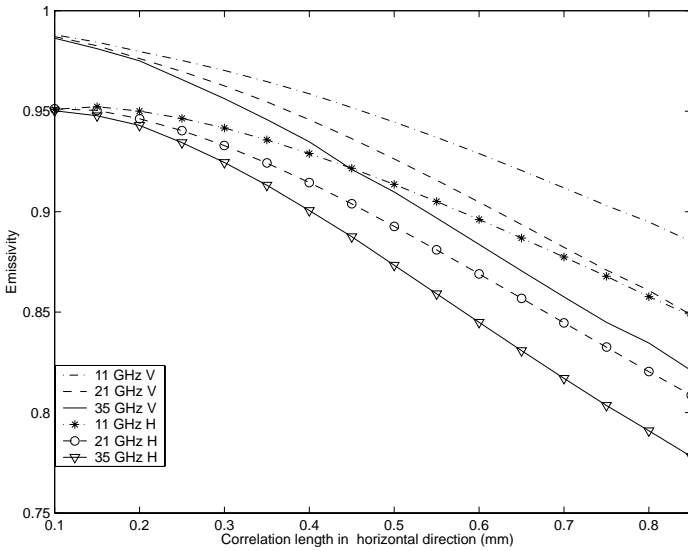
Figure 6. Theoretical wet snow emissivity as a function of the correlation length in horizontal direction l_ρ. The correlation length in vertical direction l_z is set to be 0.4 mm and the observation angle is 50°. See Table 1 for other input parameters.


Figure 7. Theoretical wet snow emissivity as a function of volume fraction of water inclusions (liquid water content). The observation angle is 50°. See Table 1 for other input parameters.
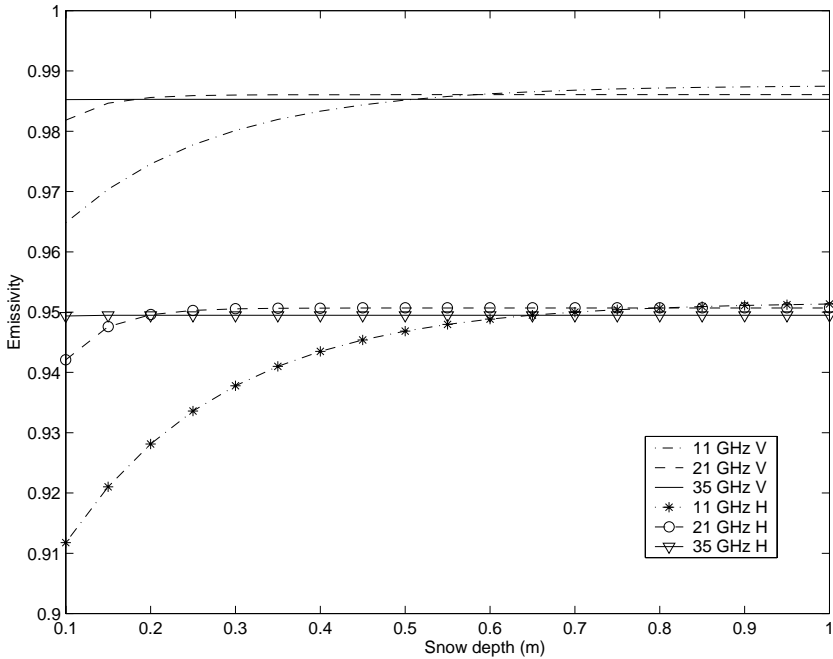
Figure 8. Theoretical wet snow emissivity as a function of snow depth. The observation angle is $50°$. See Table 1 for other input parameters.

$f_\nu \leq 0.02$, $l_z = 0.01\,\text{mm}$ and $l_\rho = 0.2\,\text{mm}$ when $f_\nu \leq 0.04$. In the calculation, water inclusions become needle-like when $f_\nu > 0.04$. The correlation lengths are selected to be $l_z = 0.43\,\text{mm}$ and $l_\rho = 0.11\,\text{mm}$ when $f_\nu > 0.04$. Figure 7 shows wet snow emissivity decreases with increasing frequency when $f_\nu \leq 0.04$. When $f_\nu > 0.04$, there are little differences in wet snow emissivity for all three frequencies. In Figure 7, the discontinuous appears when $f_\nu = 0.02$ and $f_\nu = 0.04$. This is due to we do not know details about the shape changing of water inclusions. It is clear that there is a contradiction between our results and the reference [16] about the shape of the water inclusions. This will be studied in the future.

Figure 8 shows the theoretical results of wet snow emissivity as a function of the snow depth. The observation angle is $50°$. For 21 and 35 GHz, Figure 8 indicates there are no effect on the wet snow emissivity when the snow depth change. For 11 GHz, the wet snow emissivity increase with the increasing snow depth.
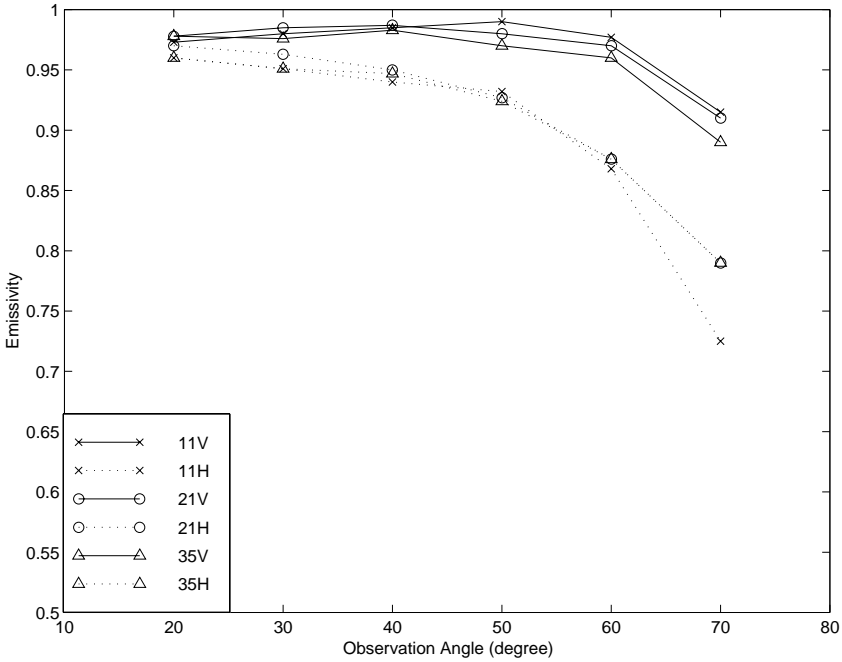
Figure 9. Observed emissivity versus incidence angle for wet snow at an Alpine test site, Weissfluhjoch, Davos, Switzerland, on June 20, 1955 [14].
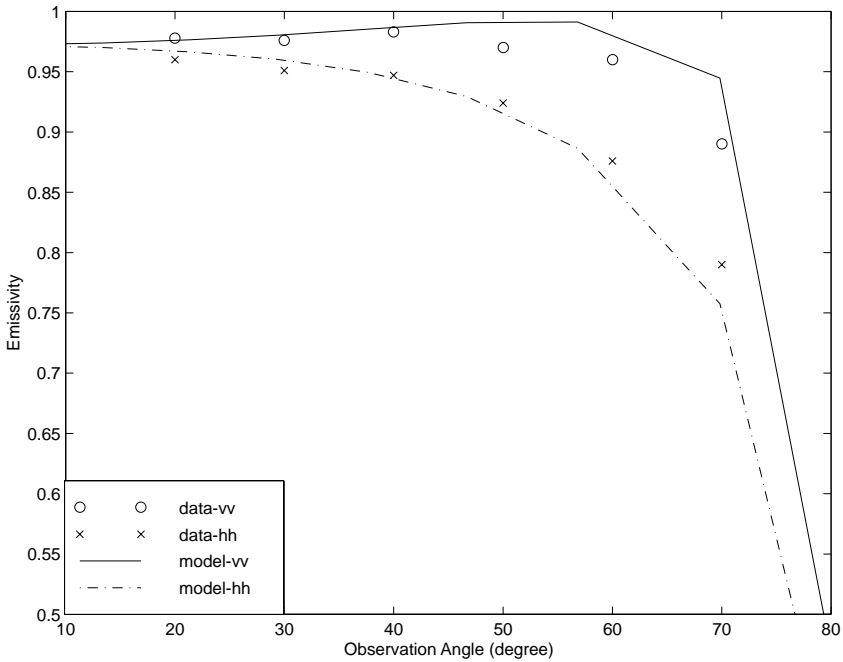
5. COMPARISON WITH EXPERIMENTAL DATA

Here we show the results for interpretation of experimental data collected for wet snow [14] by using the microwave emission model developed in this study. In [14], a set of three microwave radiometers at frequencies 11, 21 and 35 GHz was used to measure the brightness temperatures of melting snow. The observed emissivity versus incidence angle for wet snow at an Alpine test site, Weissfluhjoch, Davos, Switzerland on June 20, 1995 are shown in Figure 9. Only limited ground-truth information is given in [14]: the snow depth is 81 cm, the air temperature is $8°$ C, the snow temperature is $1°$ C at the top of snow layer, and $0.0°$ C on the ground. Wet snow in Figure 9 shows high emissivities at all frequencies. The emissivities at vertical polarisation show a maximum at $50°$ incidence angle, whereas emissivities at horizontal polarisation decrease with increasing incidence angle, as can be expected. The polarisation difference increases with decreasing
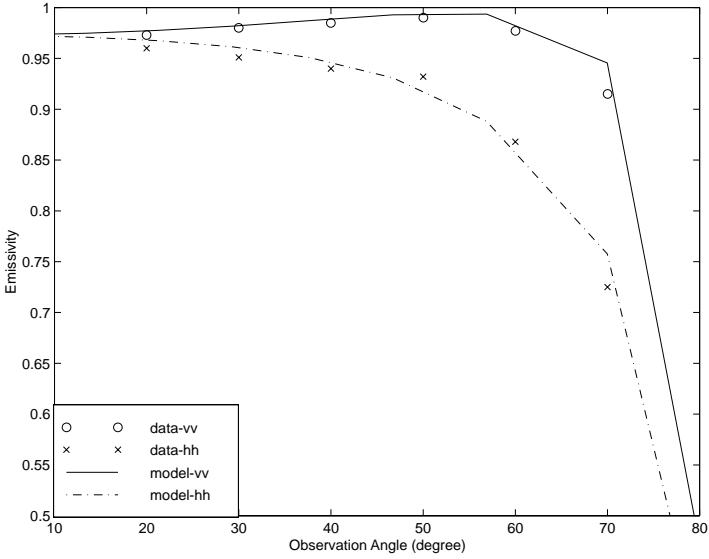
Figure 10. Comparison of the predictions from the wet snow model with experimental emissivity values given in [14] at 11 GHz. Input parameters for the theoretical model are given in Table 1.
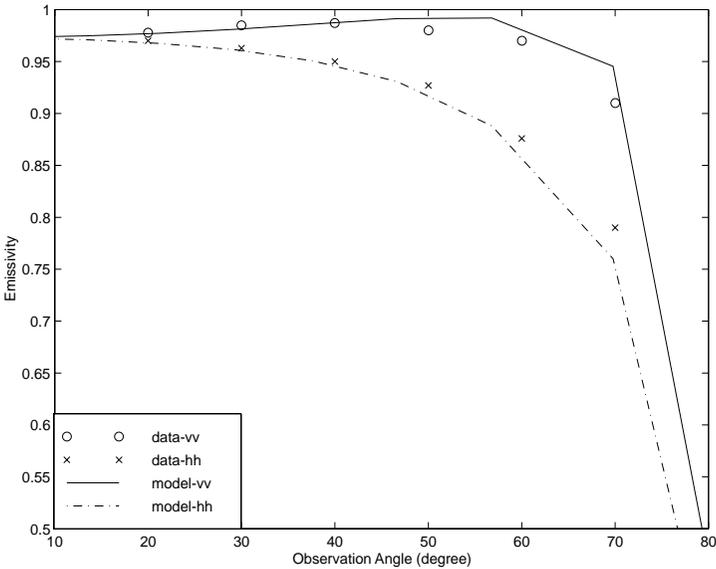
Figure 11. Comparison of the predictions from the wet snow model with experimental emissivity values given in [14] at 21 GHz. Input parameters for the theoretical model are given in Table 1.

Figure 12. Comparison of the predictions from the wet snow model with experimental emissivity values given in [14] at 35 GHz. Input parameters for the theoretical model are given in Table 1.

frequency.

The angular dependence of the emissivity was calculated by using the microwave emission model of wet snow. The input parameters are shown in Table 1. Comparisons of the predictions from the present wet snow model with experimental emissivity values given in [14] at 11, 21 and 35 GHz are shown in Figures 10 to 12, respectively. The results show that the agreement between the model predictions and measurements is good.

6. CONCLUSIONS

In this study an emission model for wet snow is derived by using radiative transfer equations and the strong fluctuation theory. The input parameters of our emission model for wet snow are the measurement frequency, the temperature of snow, the depth of snow, the mean grain size of ice particles, the volume fraction of ice particles, the volume frac-

tion of water inclusions and the correlation lengths of water inclusions in vertical and horizontal direction.

Interpretation of experimental data collected for wet snow [14] was made. It is shown that the model predictions agree well with the experimental data. The input parameters of the present microwave emission model for the values the correlation lengths of water inclusions in vertical and horizontal direction $l_\rho = 0.11\,\mathrm{mm}$ and $l_z = 0.43\,\mathrm{mm}$ provide a good match between the results of the wet snow permittivity model and the observations as well [18].

REFERENCES

1. Pulliainen, J., J. Grandell, and M. Hallikainen, "HUT snow emission mode and its applicability to snow water equivalent retrieval," *IEEE Trans. Geosci. Remote Sensing,* Vol. 37, 1378–1390, 1999.

2. Wiesman, A. and C. Mätzler, "Microwave emission model of layered snowpacks," *Remote Sensing of Environment,* Vol. 70, 307–316, 1999.

3. Stogryn, A., "A study of the microwave brightness temperature of snow from the point of view of strong fluctuation theory," *IEEE Trans. Geosci. Remote Sensing,* Vol. 24, 220–231, 1986.

4. Jin, Y. Q., "The radiative transfer equation for strongly-fluctuation continuous random media," *J. Quant. Spectrosc. Radiat. Transfer.,* Vol. 42, 529–537, 1989.

5. Wang, H., J. Pulliainen, and M. Hallikainen, "Application of strong fluctuation theory to microwave emission from dry snow," *J. Electrom. Waves and Appl.,* Vol. 14, 827–828, 2000 (abstract), and *Progress In Electromagnetic Research,* PIER 29, 39–55, 2000 (complete text).

6. Kong, J. A., R. Shin, J. Shiue, and L. Tsang "Theory and experiment for passive microwave remote sensing of snowpacks," *J. Geophys. Res.,* Vol. 48, No. B10, 5669–5673, 1979.

7. Chang, A., P. Gloersen, T. Schmugge, T. Wilheit, and H. Zwally, "Microwave emission from snow and glacier ice," *J. Glaciology,* Vol. 16, 23–39, 1976.

8. Boyarskij, D. A., V. V. Dmitriev, N. I. Kleeorin, and V. G. Mirovskij, "Theoretical and experimental studies of snow covers microwave emissivity," *J. Electrom. Waves and Appl.,* Vol. 7, 959–970, 1993.

9. Tsang, L., "Passive remote sensing of dense nonteneous media," *J. Electrom. Waves and Appl.,* Vol. 1, 159–173, 1987.

10. Tsang, L., Z. Chen, S. Oh, R. J. Marks II, and A. T. C. Chang, "Inversion of snow parameters from passive microwave remote sensing measurements by a neural network trained with a multiple scattering model," *IEEE Trans. Geosci. Remote Sensing,* Vol. 30, 1015–1024, 1992.

11. Tiuri, M. E., "Theoretical and experimental studies of microwave emission signatures of snow," *IEEE Trans. Geosci. Remote Sensing,* Vol. 20, 51–57, 1982.

12. Boyarskij, D. A. and V. S. Etkin, "Two flow model of wet snow microwave emissivity," *Proceedings of IGARSS94 Symposium,* 2068–2070, 1994.

13. Weise, T., "Radiometric and structural measurements of snow," Ph.D. Thesis, Institute of Applied Physics, University of Bern, CH-3012 Bern, Switzerland, 1996.

14. Wiesmann, A., T. Strozzi, and T. Weise, "Passive microwave signature catalogue of snow covers at 11, 21, 35, 48 and 94 GHz," *IAP Research Report,* No. 96–8, University of Bern, Switzerland, 1996.

15. Tsang, L. and J. A. Kong, "Scattering of electromagnetic waves for random media with strong permittivity fluctuations," *Radio Sci.,* Vol. 16, 303–320, 1981.

16. Hallikainen, M., F. Ulaby, and M. Abdelrazik, "Dielectric properties of snow in 3 to 37 GHz range," *IEEE Trans. on Antennas and Propagation,* Vol. 34, 1329–1340, 1986.

17. Jin, Y. Q. and J. A. Kong, "Strong fluctuation theory for electromagnetic wave scattering by a layer of random discrete scatters," *J. Applied Physics,* 55, 1364–1369, 1984.

18. Arslan, A. N., H. Wang, J. Pulliainen, and M. Hallikainen, " Effective permittivity of wet snow by using strong fluctuation theory," Submitted for publication in *J. Electrom. Waves and Appl.,* 2000.

19. Nghiem, S. V., R. Kwok, J. A. Kong, and R. T. Shin, "A model with ellipsoidal scatterers for polarimetric remote sensing of anisotropic layered media," *Radio Sci.,* Vol. 28, 687–703, 1993.

20. Nghiem, S. V., R. Kwok, S. H. Yueh, J. A. Kong, C. C. Hsu, M. A. Tassoudji, and R. T. Shin, "Polarimetric scattering from layered media with multiple species of scatterers," *Radio Sci.,* Vol. 30, 835–852, 1995.

21. Nghiem, S. V., R. Kwok, J. A. Kong, R. T. Shin, S. A. Arcone, and A. J. Gow, "An electrothermodynamic model with distributed properties for effective permittivity of sea ice," *Radio Sci.,* Vol. 31, 297–311, 1996.

22. Hallikainen, M., F. Ulaby, and T. Deventer, "Extinction behavio-

ur of dry snow in the 18- to 90-GHz range," *IEEE Trans. Geosci. Remote Sensing,* Vol. 25, 737–745, 1987.

23. Tsang, L. and J. A. Kong, "Thermal microwave emission from a three-layer random medium with three-dimensional variations," *IEEE Trans. Geosci. Remote Sensing,* Vol. 18, 212–216, 1980.

24. Stogryn, A., "The bilocal approximation for the effective dielectric constant of an isotropic random medium," *IEEE Trans. on Antennas and Propagation,* Vol. 32, 517–520, 1984.

25. Wang, H., J. Pulliainen, and M. Hallikainen, "Effective permittivity of dry snow in the 18 to 90 GHz range," *J. Electrom. Waves and Appl.,* Vol. 13, 1391–1392, 1999 (abstract), and *Progress In Electromagnetic Research,* PIER 24, 119–133, 1999 (complete text).

26. Hallikainen, M., F. Ulaby, M. Dobson, M. El-Rayes, and L. Wu, "Microwave dielectric behaviour of wet soil — Part I: empirical equations and experimental observations," *IEEE Trans. Geosci. Remote Sensing,* Vol. 23, No. 1, 25–34, 1985.

27. Hufford, G., "A model for the complex permittivity of ice at frequencies below 1 THz," *Int. J. IR and MM Waves,* Vol. 12, No. 7, 677–682, 1991.

28. Mtzler, C. and U. Wegmüller, "Dielectric properties of freshwater ice at microwave frequencies," *J. Phys. D: Appl. Phys.,* Vol. 20, 1623–1630, 1987.

29. Ulaby, F., R. Moore, and A. Fung, *Microwave Remote Sensing,* Vol. III, 2020–2022, Artech House, Inc., Norwood, MA 02062, 1986.